The Role of Magnetic Vortex Formation in Chains of Spherical FeNi Nanoparticles: A Micromagnetics Study

Prabeer Barpanda[1,2*], Michael R. Scheinfein[3], Takeshi Kasama[4,5], and Rafal E. Dunin-Borkowski[4,5]

[1]*Department of Materials Science and Engineering, Rutgers University, Piscataway, NJ 08854, U.S.A.*
[2]*Laboratoire de Réactivité et Chimie des Solides, Université de Picardie Jules Verne, CNRS UMR 6007, 33 rue Saint Leu, Amiens 80039, France*
[3]*Department of Physics, Simon Fraser University, Burnaby, BC V5A1S6, Canada*
[4]*Center for Electron Nanoscopy, Technical University of Denmark, DK-2800, Lyngby, Denmark*
[5]*Frontier Research System, The Institute of Physical and Chemical Research, Hatoyama, Saitama 350-0395, Japan*

Received January 12, 2009; accepted July 28, 2009; published online October 20, 2009

Magnetic remanent states and magnetization reversal mechanisms in linear chains of three closely-spaced $Fe_{1-x}Ni_x$ nanoparticles are studied using micromagnetic simulations, for particle sizes of between 10 and 150 nm. The role of the formation and switching of magnetic vortices in the particles is demonstrated for external fields applied parallel to the chain axes. Variations in vortex core diameter, coercivity and vortex rotation plane with applied field are discussed. © 2009 The Japan Society of Applied Physics

DOI: 10.1143/JJAP.48.103002

1. Introduction

A detailed understanding of the magnetic properties of closely-spaced, strongly interacting ferromagnetic particles is important in order to gain a fundamental understanding of the nucleation and propagation of vortices in nanometer-sized ferromagnets, and, from a technological perspective, to gain insight into the design of three-dimensional nanoscale magnetic devices. Here, we use micromagnetic simulations to examine the formation and reversal of three-dimensional magnetic vortex states in well-defined systems of short chains of ferromagnetic spheres. These chains of nanosphere systems can be helpful in simulating magnetic nanostructures like ferromagnetic ellipsoids and nanorods/nanowires. Magnetization reversal mechanisms in linear chains of spherical particles containing single magnetic domains were originally discussed by Jacobs and Bean,[1)] who used their calculations to account for unexpectedly low coercivities measured from elongated fine particles. Since then, the chain-of-sphere model has been used to describe experimental observations on nanoparticulate chains with smaller particles containing single domains.[2–4)] Also, the chain-of-sphere model with single-domain nanoparticles has been theoretically studied.[5,6)] However, there is a dearth of literature on experimental/theoretical investigation on nanoparticulate chains with larger spheres supporting multiple-domains.[7)] The present study is motivated by the direct observation of magnetic vortex states in chains of $Fe_{1-x}Ni_x$ particles of average diameter 50 nm using electron holography.[8,9)] Experimentally, both the vortex core diameters and the critical sizes at which particles in the chains ceased to be single domain at remanence were observed to increase with exchange length, as particles of increasing Ni concentration were examined. In the simulations described below, the formation and switching of vortices in such particles is demonstrated for external fields applied parallel to the chain axis. Variations in vortex core diameter, coercivity and vortex rotation plane with applied field are also discussed. The current paper is our first step to investigate the chain-of-sphere systems that contain larger supporting magnetic vortices.

*E-mail address: prabeer.barpanda@u-picardie.fr

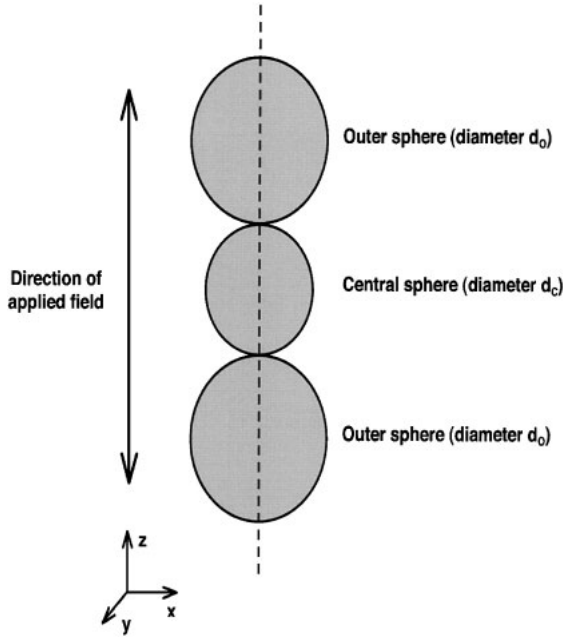

Fig. 1. Geometry of the linear chain of three spheres. The central sphere has diameter d_C, the outer spheres have diameters d_O, and external fields are applied parallel to the chain axis. The chain axis lies parallel to the z axis.

2. Simulation Details

Simulations of magnetization reversal in linear chains of three spheres were carried out for sphere diameters between 10 and 150 nm by solving the Landau–Lifshitz–Gilbert (LLG) equations in the continuum micromagnetic limit using LLG software.[10)] The geometry of the chain of spheres, whose axis is defined to lie along z, is shown schematically in Fig. 1. The three spheres were modeled using discrete moments, with the demagnetization field computed to all orders. The simulation mesh used cubic cells 2 nm on a side to capture the nucleation, propagation and annihilation of magnetic vortices. With this simulation mesh, smaller spheres (size, $d < 50$ nm) share one mesh, whereas larger sphere (size, $d > 50$ nm) share nine meshes with neighbouring spheres. The number of contact meshes

Table I. Input material properties. M_S is the saturation magnetization and A is the exchange stiffness.

	M_S (emu/cm^3)	A (μerg/cm)
Fe	1714	2.10
$Fe_{56}Ni_{44}$	1273	1.13
$Fe_{20}Ni_{80}$	800	1.05
Ni	484	0.80

among spheres is pivotal as it affects their exchange coupling. To ensure our meshing was correct to simulate spheres with point contact, some initial simulations were performed with extremely small mesh size of 0.5–1 nm to ensure just 1 mesh contact between neighbouring spheres. Similar results were observed. A gyromagnetic frequency γ of 17.6 MHz/Oe and a damping constant α of 1 were used, as only equilibrium states were considered. The effects of thermal fluctuations were not included. The exit criterion for computing equilibrium magnetization distributions was triggered by the largest residual direction cosine of the moments in the grid changing by less than 10^{-4}. Magnetization reversal mechanisms were investigated by applying external fields of between −8000 and +8000 Oe parallel to the chain axes. Spheres of Fe, $Fe_{56}Ni_{44}$, $Fe_{20}Ni_{80}$, and Ni were studied, using the input parameters listed in Table I. The time step used in the calculations was 4 ps, and the results presented below were found to be independent of both the direction of magnetocrystalline anisotropy and the initial magnetization state included in the calculations.

3. Results and Discussion

3.1 Magnetic remanent states

Schematic diagrams that illustrate the magnetic single domain and vortex states that were observed at remanence using the LLG simulations are shown in Fig. 2. The critical size at which each particle was able to support a vortex state depends not only on its composition and size, but also on its position in the chain and on the sizes of the neighboring particles. Depending on the relative sizes of the particles, a vortex in the central particle in the chain can be stabilized by the presence of single domain states in the outer particles, or conversely a single domain state can be stabilized by the presence of vortices in the outer particles. Results of micromagnetic simulations, showing the transition between the formation of single domain and vortex states at remanence in the central particle, are shown in Figs. 3(a) and 3(b) for chains of Fe and Ni, respectively. In both cases, the diameter at which the central particle begins to support a vortex state increases steadily as the diameters of its neighbors increase. This stabilization of a single domain state in the central particle results from the channeling of magnetic flux from the central particle to the vortex cores in the outer particles, which themselves increase in width with particle diameter. The step seen in each diagram in Fig. 3(a) occurs below the diameter at which the outer particles begin to support vortex states, and is associated with the stabilizing effect of single domain states in the particles at the ends of the chain on the formation of a vortex state in the central particle, in particular when their diameter is comparable to

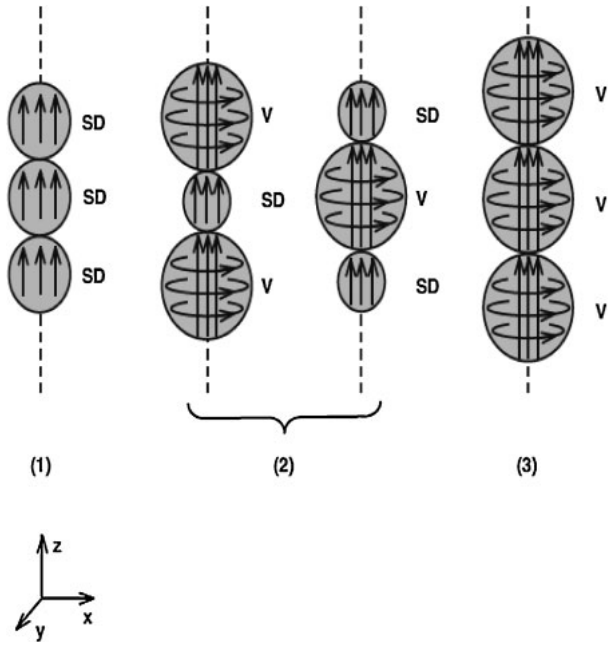

Fig. 2. Schematic diagrams showing the different magnetic remanent states observed in the linear chains of three spheres using micromagnetic simulations. SD and V refer to single domain and vortex states, respectively. The chain axes lie parallel to the z axis.

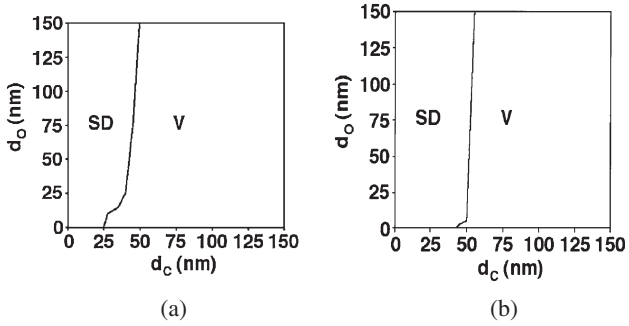

Fig. 3. Results of micromagnetic simulations, showing the magnetic remanent states that form in the central sphere in a chain of three spheres of (a) Fe and (b) Ni, plotted as a function of both the central sphere diameter d_C and the outer sphere diameters d_O. SD and V refer to single domain and vortex states, respectively.

or smaller than that of the vortex core. The increase in exchange length in the Ni particles [Fig. 3(b)] from that in the Fe particles [Fig. 3(a)] results in the stability of single domain states to larger particle diameters. The step in Fig. 3(b) is less prominent than in Fig. 3(a), indicating that for Ni particles only the smallest single domain outer particles are able to stabilize a vortex state significantly in the central particle.

3.2 Magnetization reversal mechanisms

In the original chain-of-sphere model having single-domain nanospheres proposed by Jacobs and Bean,[1)] standard reversal mechanisms such as fanning, parallel rotation and curling were mentioned. However, in our system, magnetization reversal mechanisms in the particles involved either single domain switching [Fig. 4(a)] or the formation and annihilation of vortex states [Fig. 4(b)], depending on their diameter and composition. During vortex formation in larger

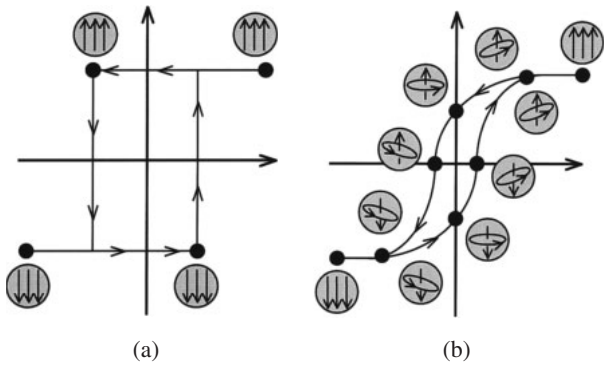

Fig. 4. Schematic diagrams, based on the results of micromagnetic simulations, showing the evolution of magnetic states during magnetization reversal in (a) isolated spheres that contain single domains and (b) isolated spheres that are large enough to support vortices. The external field is applied in the vertical direction (along the *z* axis).

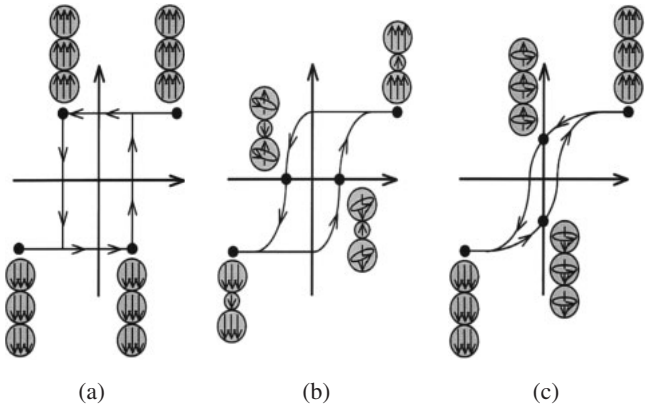

Fig. 5. Schematic diagrams showing the evolution of magnetic states, observed using micromagnetic simulations, during magnetization reversal in (a) chains of three spheres that contain only single domains, (b) chains of three spheres in which the diameter of the central sphere is very different from that of the outer spheres, and (c) chains of three spheres that are large enough to support vortices. The external field is applied in the vertical direction (along the *z* axis). The reversal mechanisms are referred to as (a) domain switching (DS), (b) hybrid reversal (HR), and (c) vortex creation and annihalation (VCA).

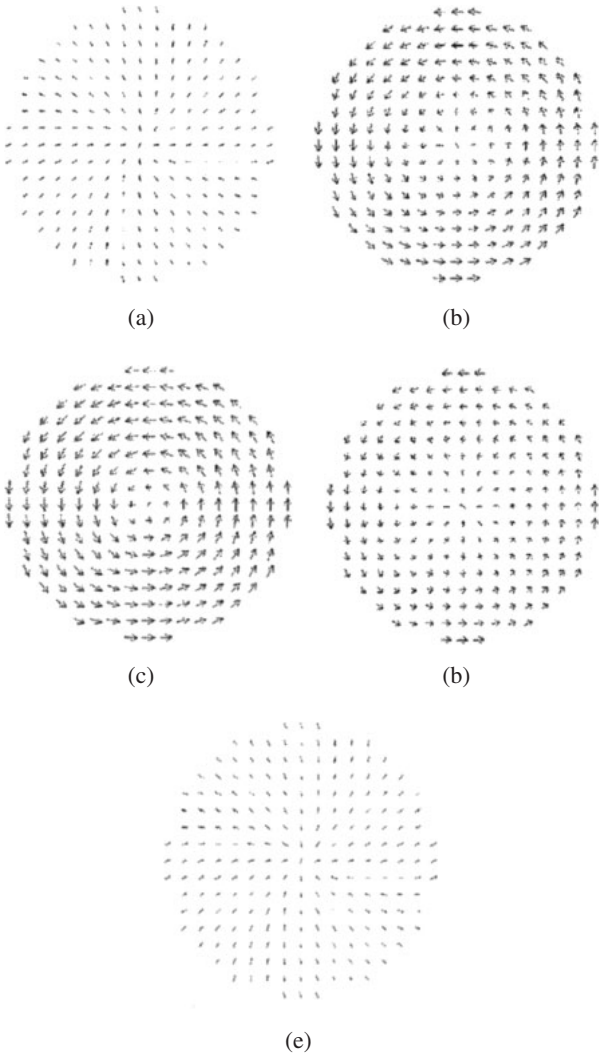

Fig. 6. Representative results from micromagnetic simulations showing vortex creation and annihalation in the central sphere of a chain of three spheres. The calculation was carried out for a chain of Ni spheres, with a central sphere of diameter d_C of 100 nm and outer sphere diameters d_O of 30 nm. The applied fields along the chain axis are (a) 3200, (b) 1600, (c) 0, (d) −1600, and (e) −3200 Oe. The arrows in the figures show the strength and direction of the magnetic induction in the *x*–*y* plane (perpendicular to the chain axis) at the centre of the chain.

particles, a saturated magnetic state in a large external field transformed into a helical vortex, in which a significant component of the moment surrounding the core was in the direction of the applied field. At remanence, the moments surrounding the core were exactly perpendicular to the applied field direction, while in a reverse field a helical vortex state again formed, with the same chirality as in the first part of the cycle. With increasing reverse field, the direction of the vortex core reversed, and finally a saturated state formed. During the second half of the cycle, the chirality of the vortex core was always the same as in the first half of the cycle. Three particles in a chain either behaved similarly to each other during reversal [Figs. 5(a) and 5(c)] or underwent a hybrid reversal process, in which the central particle reversed by single domain switching and the neighboring particles by the formation of vortices, or *vice versa* [Fig. 5(b)]. It should be noted that, in contrast to the "fanning" of single domain states expected when an external field is applied at an angle to the axis of a chain of small particles,[1)] chains in which the particles were too small to support vortices switched their magnetization direction at a single value of the applied field and always gave rise to square hysteresis loops [Fig. 5(a)]. Representative results from an LLG simulation are shown in Fig. 6. The calculation illustrates, in the form of arrows, the magnetic induction in the *x*–*y* plane (perpendicular to the chain axis) in the middle of the central sphere of a chain of three Ni spheres during the creation and annihilation of a vortex, for a central sphere diameter d_C of 100 nm and outer sphere diameters d_O of 30 nm. The diameters of the central and outer spheres in the chains at which the three different magnetization reversal mechanisms are active are summarized in Fig. 7 for all four compositions. Qualitatively, single domain switching (DS) occurs for the smallest central and outer sphere diameters, vortex creation and annihilation (VCA) for the largest central and outer sphere diameters, and hybrid reversal (HR) when spheres that are sufficiently large but have different diameters are combined in the same chain.

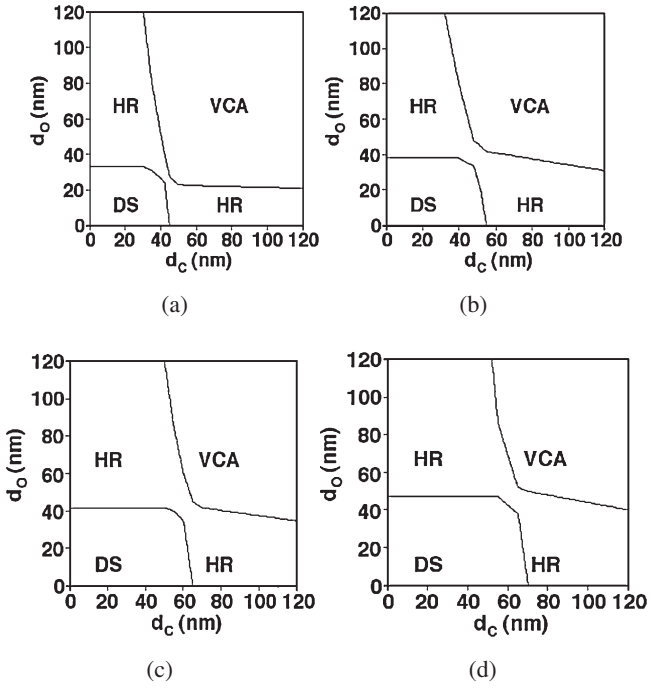

Fig. 7. Results of micromagnetic simulations showing the magnetization reversal mechanisms that are observed in chains of three spheres of (a) Fe, (b) $Fe_{56}Ni_{44}$, (c) $Fe_{20}Ni_{80}$, and (d) Ni, plotted as a function of both the central sphere diameter d_C and the outer sphere diameters d_O. DS, HR, and VCA refer to single domain switching, hybrid reversal and vortex creation and annihalation, respectively, as described in the form of schematic diagrams in Fig. 5.

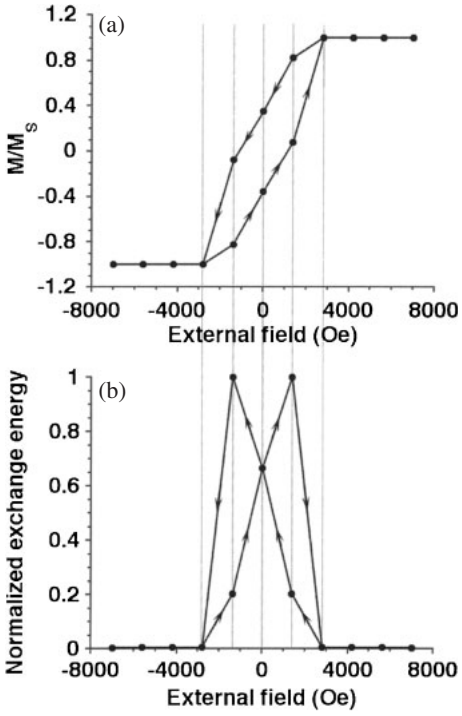

Fig. 8. Representative results from micromagnetic simulations showing (a) a hysteresis loop and (b) the variation in exchange energy in a chain of three spheres during magnetization reversal. The calculation was carried out for a chain of Fe spheres, with a central sphere diameter d_C of 50 nm and outer sphere diameters d_O of 75 nm.

An increase in Ni content (and hence exchange length) stabilizes single domain switching to larger diameters. In all of the graphs shown in Fig. 7, single domain switching in the central sphere is stabilized to larger diameters by the presence of either small or large outer spheres, resulting in the asymmetry visible about the diagonal of each graph.

3.3 Exchange energy, vortex core diameter, and vortex rotation plane

Figure 8 shows a representative graph of the variation in exchange energy in a chain of three $Fe_{56}Ni_{44}$ spheres during magnetization reversal, plotted as a function of external field for a central sphere diameter d_C of 50 nm and outer sphere diameters d_O of 75 nm. The corresponding hysteresis loop for the chain is also shown. Both graphs are consistent with the presence of a uniformly magnetized state in each sphere at high fields, and with the formation and subsequent annihilation of a vortex below a certain value of the external field. The sensitivity of the diameter of the vortex core to the external field was quantified from simulations of the z-component of the magnetization in the central sphere M_Z. The vortex core diameter is important because it affects the strength of the magnetic interaction between each sphere and its neighbors, and can therefore change the magnetization reversal mechanism. The core diameter was defined as the total distance in the central sphere, over which M_Z decreases to half of its peak value in the x direction at $z = 0$, as shown in Fig. 9. The variation in core diameter with applied field in the central sphere of a chain of three $Fe_{20}Ni_{80}$ spheres is shown in Fig. 10, for a central sphere of diameter d_C of 75 nm and outer sphere diameters d_O of 100 nm. The increase in vortex core diameter with applied field seen in Fig. 10 is likely to be an important factor in stabilizing single domain switching in the central sphere in the graphs shown in Fig. 7. It should be noted that distances and positions in Figs. 9 and 10 are plotted in units of exchange length $l_{ex} = (A/2\pi M_S^2)^{1/2}$, where A is the exchange stiffness and M_S is the saturation magnetization, as the exchange length is the natural length scale that determines the underlying physics in the present problems. In Fig. 9, the exchange length takes a value of 3.4 nm for Fe, and the central sphere has a diameter of $14.8l_{ex}$. In Fig. 10, the exchange length takes a value of 5.1 nm for $Fe_{20}Ni_{80}$, and the central sphere has a diameter of $14.7l_{ex}$.

The spiraling of the vortex in the central sphere can be quantified by measuring the angle of the moments in the vortex from the x–y plane. Although this angle changes smoothly from the center of the sphere to its edge, rather than abruptly at the edge of the vortex core, an assessment of its magnitude can be obtained at a fixed radius in the mid-plane of the sphere (the x–y plane at $z = 0$). Results showing values of this angle measured from LLG simulations are shown in Fig. 11, for a chain of three $Fe_{20}Ni_{80}$ spheres with a central sphere diameter d_C of 75 nm and outer sphere diameters d_O of 100 nm. In Fig. 11, the angle of the vortex rotation plane is measured at a radius of half of that of the sphere (at $z = 0$). It can be seen from Fig. 11 that the moments can reach angles from the x–y plane in excess of 40°. The fact that the canting may be unstable beyond 45° is interesting, implying either that the energy surface is metastable or that the energy surface slope becomes much larger at this value of applied field.

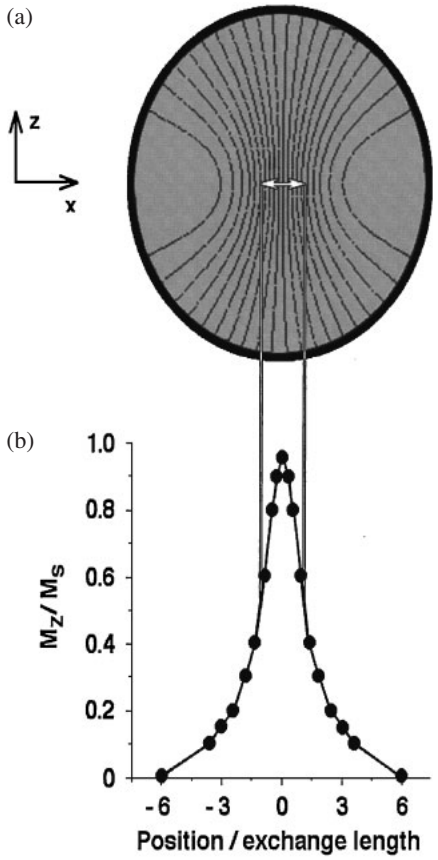

Fig. 9. Representative result from a micromagnetic simulation showing the approach used to measure the vortex core diameter in the central sphere of a chain of three spheres. (a) shows contours in the x–z plane in the central sphere, generated from the calculated z-component of the magnetization M_Z, where z is the chain axis, for a chain of Fe spheres with a central sphere diameter d_C of 50 nm and outer sphere diameters d_O of 75 nm. (b) shows the value of M_Z plotted across the diameter of the sphere. The horizontal axis of the graph is shown in units of exchange length, which takes a value of 3.4 nm for Fe. The vortex core diameter is measured from the full width at half maximum of this plot.

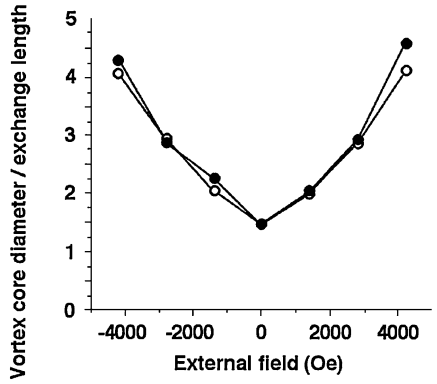

Fig. 10. Results from a micromagnetic simulation showing the vortex core diameter in the central sphere of a chain of three spheres measured during magnetization reversal. The solid and open circles represent decreasing and increasing fields, respectively. The calculations were carried out for a chain of $Fe_{20}Ni_{80}$ spheres with a central sphere of diameter d_C of 75 nm and outer sphere diameters d_O of 100 nm. The vortex core diameter is shown in units of exchange length, which takes a value of 5.1 nm for $Fe_{20}Ni_{80}$.

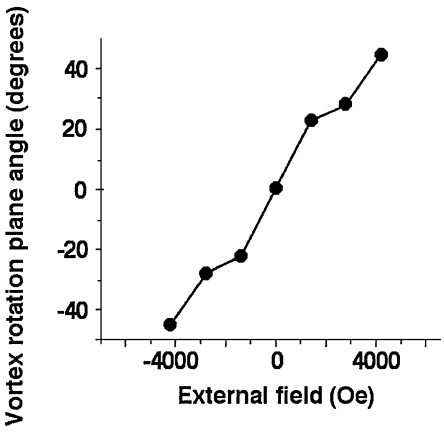

Fig. 11. Results from a micromagnetic simulation showing the angle of the vortex rotation plane from the x–y plane of the central sphere of a chain of three spheres, measured during magnetization reversal at $z = 0$. The calculations were carried out for a chain of $Fe_{20}Ni_{80}$ spheres with a central sphere of diameter d_C of 75 nm and outer sphere diameters d_O of 100 nm. The angle is measured at a distance of half of the radius of the sphere from its center.

3.4 Coercivity and remanence

The reversal mechanisms described above are related intimately to the coercivity and remanence of each chain. Graphs of the calculated coercivity are shown in Fig. 12 for all four compositions and for different sphere diameters. Although the details are clearly complicated, and the limited number of data points may obscure some of the features in the graphs, some trends can be identified. The coercivity of each chain is highest for the smallest sphere sizes, which undergo single domain switching.[11,12] Most of the features in the graphs result from the fact that vortex creation and annihilation, either in the central sphere or in the outer spheres, result in lower values of coercivity. Not only does a larger sphere diameter result in lower coercivity, but the presence of a larger sphere is likely to initiate the reversal process in a chain. The higher coercivities observed for higher Ni contents result from the greater proportion of the simulations in which single domain switching takes place.

The squareness of each hysteresis loop (the remanent magnetization M_R divided by the saturation magnetization M_S) is also governed by the magnetization reversal mechanism. Figure 13 shows values of squareness (M_R/M_S) calculated for chains of three spheres of $Fe_{20}Ni_{80}$. In broad agreement with the coercivities shown in Fig. 12, the squareness of the chain of spheres is unity for smaller spheres, which reverse by single domain switching [as in Fig. 5(a)]. When either the center or the outer sphere supports a vortex at remanence, the squareness decreases.

4. Conclusions

Simulations of magnetic remanent states and magnetization reversal mechanisms in linear chains of three FeNi spheres have been presented. The coercivity and the remanence of each chain decrease as a result of the creation and annihilation of vortices, whether these vortices form in the central or the outer spheres. As a result of a delicate balance between the long-range demagnetization field of the particles and the local exchange energy, any of the spheres in a chain can set the nucleation threshold for switching or

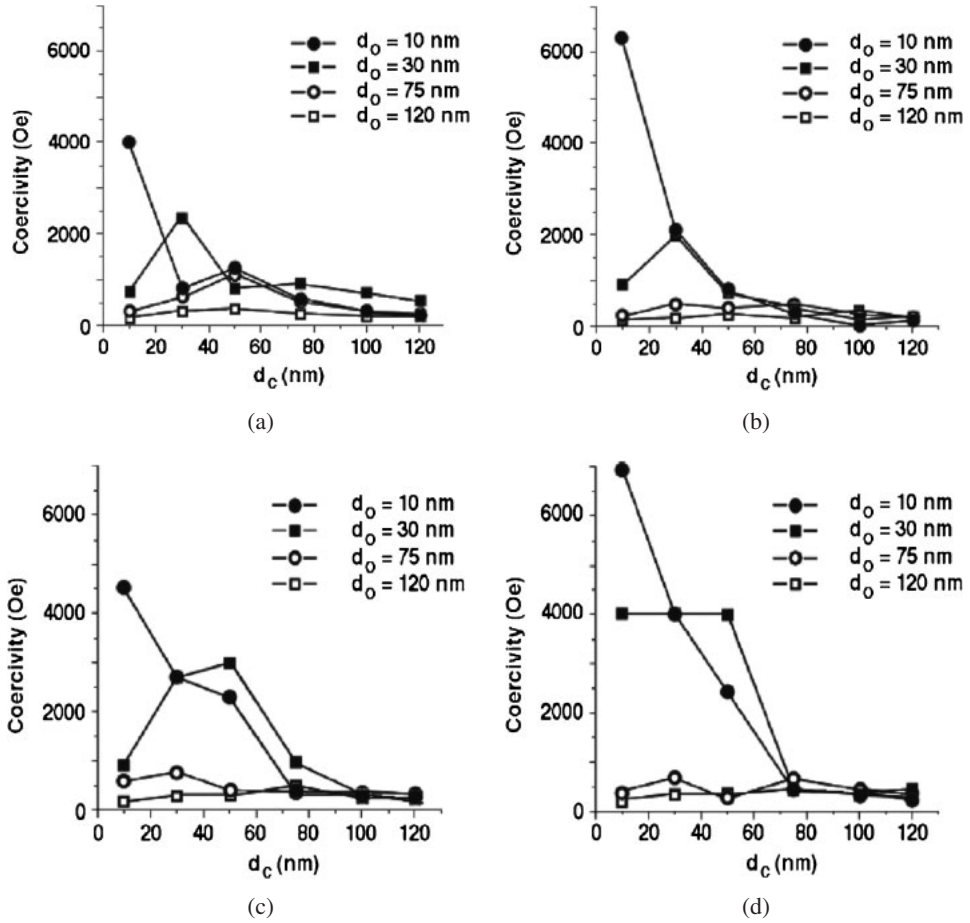

Fig. 12. Results of micromagnetic simulations showing the coercivities of chains of three spheres of (a) Fe, (b) $Fe_{56}Ni_{44}$, (c) $Fe_{20}Ni_{80}$, and (d) Ni, plotted as a function of central sphere diameter d_C for a range of outer sphere diameters d_O.

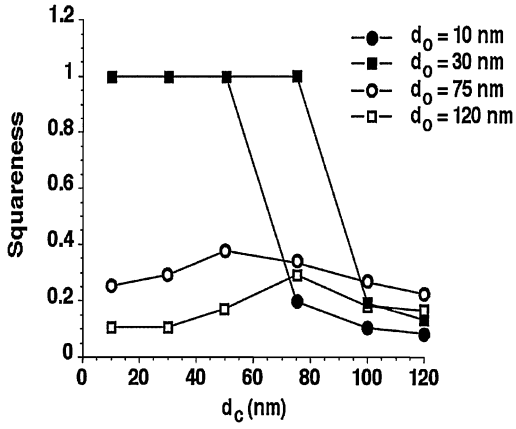

Fig. 13. Values of squareness (M_R/M_S) calculated for chains of three spheres of $Fe_{20}Ni_{80}$, plotted as a function of central sphere diameter d_C for a range of outer sphere diameters d_O.

present an energy barrier to that switch. The energy barrier for nucleation and switching is affected by the degeneracy of the observed magnetic states, including the helicity of the vortices and the rotation plane of the magnetization about these vortices.[13] Even in the present limited and simple model, with ideal spheres of fixed symmetry, the switching behavior is fascinating due to the degrees of freedom that are available to three-dimensional objects that are in close proximity to each other.

Acknowledgement

The current paper is an outcome of M. Phil. dissertation in Materials Modeling at the Department of Materials Science and Metallurgy, University of Cambridge. PB is grateful to the Cambridge Commonwealth Trust for a Shell Centenary Chevening Scholarship at Cambridge and NSF IMI Program (award # DMR04-09848). We thank N. D. Mathur, B. B. van Aken, M. J. Hÿtch, and R. J. Harrison for technical discussions.

1) I. S. Jacobs and C. P. Bean: Phys. Rev. **100** (1955) 1060.
2) Y. Peng, H. Zhang, S. Pan, and H. Li: J. Appl. Phys. **87** (2000) 7405.
3) L. Zhang and A. Manthiram: Phys. Rev. B **54** (1996) 3462.
4) K. H. Lee, H. Y. Lee, W. Y. Jeung, and W. Lee: J. Appl. Phys. **91** (2002) 8513.
5) A. Aharoni: J. Appl. Phys. **35** (1964) 347.
6) A. Aharoni: J. Appl. Phys. **82** (1997) 1281.
7) P. Barpanda: Comput. Mater. Sci. **45** (2009) 240.
8) M. J. Hÿtch, R. E. Dunin-Borkowski, M. R. Scheinfein, F. Mazaleyrat, and Y. Champion: Phys. Rev. Lett. **91** (2003) 257207.
9) R. K. K. Chong, R. E. Dunin-Borkowski, T. Kasama, M. J. Hÿtch, and M. R. McCartney: Inst. Phys. Conf. Ser. **179** (2003) 451.
10) http://llgmicro.home.mindspring.com
11) R. Gunnarsson, M. Hanson, and C. Dubourdieu: J. Appl. Phys. **96** (2004) 482.
12) A. Magni, G. Bertotti, and I. Mayergoyz: J. Appl. Phys. **89** (2001) 7451.
13) F. Porrati and M. Huth: Appl. Phys. Lett. **85** (2004) 3157.